Effect of the anisotropic surface tension, crystallization kinetics, and heat diffusion on nonequilibrium growth of liquid crystals

T. Börzsönyi and Á. Buka
Research Institute for Solid State Physics and Optics, Hungarian Academy of Sciences, P.O.B. 49, H-1525 Budapest, Hungary

L. Kramer
Institute of Physics, University of Bayreuth, D-95440 Bayreuth, Germany
(Received 3 December 1997; revised manuscript received 31 July 1998)

The morphologies of a homeotropic smectic-*B* germ growing into an undercooled homeotropic or planar nematic melt were studied. The two sets of growth shapes observed in the experiment were reproduced by computer simulations using a phase-field model. From the comparison of the experiment and numerical simulations we give an estimate for the anisotropy of the surface tension and the kinetic coefficient for the case of the homeotropic nematic melt. In the case of the planarly aligned melt the twofold anisotropy of the nematic superimposes onto the hexagonal symmetry of the smectic *B*. An explanation of the phenomenon of the ''inverted growth'' is given. [S1063-651X(98)09511-7]

PACS number(s): 81.10.Aj, 61.30.−v, 64.70.Md

I. INTRODUCTION

The solidification of a simple, pure substance through free growth of a crystalline germ into its melt is a well-studied process which leads to interfacial patterns [1]. In the usual description one considers a temperature field $T(\mathbf{r},t)$ which satisfies the diffusion equation (1.1) on both sides of the moving sharp interface separating the two phases. The normal velocity of the interface v_n is determined from the heat conservation condition (1.2) together with the Gibbs-Thomson relation (1.3), which involves the angular dependent surface tension $\sigma(\theta)$ and a linear kinetic term $\beta(\theta)v_n$, where θ is the angle between the surface normal and a reference direction — the x axis. We consider a two-dimensional system in the xy plane.

$$\frac{\partial T}{\partial t}=D\nabla^2 T, \tag{1.1}$$

$$Lv_n=D^{\text{solid}}c_p^{\text{solid}}(\boldsymbol{\nabla}_n T)_{\text{solid}}-D^{\text{liquid}}c_p^{\text{liquid}}(\boldsymbol{\nabla}_n T)_{\text{liquid}}, \tag{1.2}$$

$$T_{\text{interface}}=T_m-\frac{T_m}{L}[\sigma(\theta)+\sigma''(\theta)]\kappa-\beta(\theta)v_n. \tag{1.3}$$

The parameters are T_m — melting temperature, L — latent heat per unit volume, c_p — specific heat per unit volume, D — heat diffusion coefficient, and κ — the local curvature of the interface. The undercooling $\Delta T=T_m-T_\infty$ enters as a boundary condition (T_∞ is the temperature far away from the germ).

Since in the usual growth process the germ remains practically isothermal at T_m, the heat current in the solid phase [the first term on the right hand side of Eq. (1.2)] is small compared to that in the liquid phase. For this reason the growth process is rather insensitive to the precise values of D^{solid} and c_p^{solid}. Thus, for simplicity, we use everywhere the material parameters of the liquid phase. As usual, any temperature dependence of the material parameters is neglected. This could become problematic when the type of transition becomes only weakly first order, which is probably not the case here.

It is useful to introduce dimensionless parameters by scaling lengths in some arbitrary reference length ω (usually chosen of the order of the size of the well-developed germ), while times are scaled by ω^2/D. The angular dependence of the surface tension and that of the kinetic coefficient is separated from their angular averages (σ_0 and β_0) by writing

$$\sigma(\theta)=\sigma_0\tilde{\sigma}(\theta),\quad \beta(\theta)=\beta_0\tilde{\beta}(\theta). \tag{1.4}$$

With $u(\mathbf{r},t)=(T-T_m)/\Delta T$ one then has

$$\frac{\partial u}{\partial t}=\nabla^2 u, \tag{1.5}$$

$$v_n=[(\boldsymbol{\nabla}_n u)_{\text{solid}}-(\boldsymbol{\nabla}_n u)_{\text{liquid}}]\Delta, \tag{1.6}$$

$$u_{\text{interface}}=-\frac{\sqrt{2}}{12\alpha\Delta}\{[\tilde{\sigma}(\theta)+\tilde{\sigma}''(\theta)]\kappa+\tau_0\tilde{\beta}(\theta)v_n\}. \tag{1.7}$$

The dimensionless parameters of the system are

$$\Delta=\frac{c_p\Delta T}{L}, \tag{1.8}$$

$$\alpha=\frac{\sqrt{2}\omega L^2}{12c_p\sigma_0 T_m}=\frac{\sqrt{2}\omega}{12d_0}, \tag{1.9}$$

$$\tau_0=\frac{LD\beta_0}{T_m\sigma_0}. \tag{1.10}$$

In the following we give a brief survey of the literature concentrating on the effect of the *anisotropies* of the material parameters on the pattern formation. From analytical and numerical studies of the sharp interface model [Eqs. (1.5)–

(1.7)], or simplified versions thereof, see, e.g., [2], it is well known that the angular dependence of $\tilde{\sigma}$ and $\tilde{\beta}$ plays a crucial role in stabilizing dendritic (or needle crystal) growth. In the case of *surface tension* dominated growth a comparison between experiment and theory (microscopic solvability) restricted to small surface tension anisotropies was carried out with conventional materials (pivalic acid and succinonitrile) by analyzing the shape of growing dendritic tips [3–7]. The surface tension anisotropy can be determined experimentally by analyzing the equilibrium shape of the interface. The magnitude of the anisotropy was reported for ice [6], pivalic acid (PVA) [7,8], NH_4Br [9], succinonitrile (SCN) [7], camphene [3], and for ^{4}He crystals [10,11]. The influence of the *kinetic coefficient* has been analyzed less, see, e.g., [12]. Experimental studies were done on ammonium chloride [13] and in particular using liquid crystals (see below). The effect of the *anisotropic heat diffusion* in the liquid phase (which is also a specific feature of the liquid crystalline systems) to our knowledge was first analyzed in [14].

As a result of the varying influence of noise, surface tension, and kinetic effects one finds as a function of undercooling morphological transitions. The resulting morphology diagrams have been studied by various theoretical approaches [15–22].

In liquid crystalline phase transitions the effect of the anisotropies on the pattern formation can be studied in a quite broad range, see, e.g., [23]. The morphology diagram was reported and experimental results on both the surface tension and kinetic anisotropy have been given for columnar hexagonal liquid crystals [24,25]. In the smectic to crystal phase transition the morphological transitions and the nature of mode selection were analyzed [26]. The morphology diagram was also studied for very large twofold anisotropies of the surface tension in the nematic–smectic-B phase transition experimentally [27–29] and numerically [27,29] as well.

In the present paper we report on experimental and numerical (using a phase-field model) results on the morphology of the interface of a smectic-B germ growing into a nematic melt. This phase boundary has a very weak surface tension anisotropy and kinetic anisotropy in the two arrangements investigated: homeotropic smectic B in homeotropic (HinH) and in planar (HinP) nematic.

In the HinH case we give an estimate of the sixfold anisotropy of the surface tension and kinetic coefficient based on the numerical reproduction of the experimentally observed morphologies.

In the HinP case the effect of the anisotropies on the pattern formation becomes a more complex problem. The new features (compared to a crystal-liquid interface) originate from the additional anisotropy of the surrounding melt, which is in our case the uniaxial nematic liquid crystal. Both angular functions $\tilde{\sigma}(\theta)$ and $\tilde{\beta}(\theta)$ will be affected by the nematic ordering, moreover the anisotropic heat diffusivity causes a higher velocity in the direction of the low heat diffusion (''inverted growth'') which we explain here with numerical and analytical methods.

The investigated HinH and HinP geometries are different from the well-studied PinP and PinH arrangements [27–29] where the surface tension anisotropy is orders of magnitude larger.

II. DESCRIPTION OF THE EXPERIMENT

Quasi-two-dimensional liquid crystal cells with thickness of 10 μm were used for investigation. By an appropriate treatment of the surface of the substrates homogenous planar or homeotropic initial alignment of the nematic director ($\mathbf{n}_N$) was achieved. The cell was placed in a temperature controlled stage which had an accuracy of ± 3 mK. The characteristic thermal response/relaxation time of our experimental system was basically determined by the heat conductivity of the glass plates and the heat capacity of the metal block in the hot stage. The exponential relaxation time was measured and a typical value of a few tens of seconds was found. This means that for the small undercoolings we mostly used, the temperature field applied can be regarded as nearly steplike on the scale of the typical growth time of a germ. This is certainly valid in the HinP case, where the growth is slower. In the HinH geometry for the two highest undercoolings ($\Delta T = 0.3$ and 0.35) this could lead to a small temperature lag at the beginning of the growth which diminishes during the process.

The commercial (MERCK—ZLI 1185) substance CCH5 (4-*n*-pentyl-4′-cyano-*trans* 1,1-bicyclohexane) we used has a first-order nematic–smectic-B phase transition at $T_m = 51.2$ °C with latent heat $L = (17 \pm 1)10^3$ J/kg. To characterize the sample purity we determined the two-phase coexistence temperature region, which was found to be in all cells less than 0.3 °C. In order to estimate the heat diffusion anisotropy $D_a = (D_\parallel - D_\perp)/D_\perp$ we took literature data measured for substances of very similar molecular structure (5CB and 8CB) for which the value of $D_a \approx 0.7$ was found [30,31] (here $D_\parallel$ and $D_\perp$ denotes the heat diffusion coefficient in the nematic phase parallel and perpendicular to the director, respectively). Preliminary measurements [32] carried out very recently on CCH5 show that here the value of D_a is even larger. No pronounced dip in $D_\perp$ (or $D_\parallel$) was found at T_m, contrary to the case of the N–S_A transition where a dip was observed [31,33–35]. For references and more details regarding the material parameters see [27].

We mention that the anisotropy of the heat diffusion was also measured for smectic phases and no significant effect of the long range smectic order was found [36].

The preparation of homeotropic germs in the homeotropic nematic is not especially difficult since in the case of CCH5 some of the smectic germs nucleate spontaneously with this orientation. As reported in [27] the orientation of the smectic germs is usually planar in the planar cell. In order to prepare homeotropic smectic germs in the planar cell one has to apply some external field, i.e., electric. If a sufficiently large ($E > 10^6$ V/m) electric field is switched on in the direction perpendicular to the substrates during the melting of the smectic phase, the nematic director realigns (the dielectric anisotropy of the substance is strongly positive) and becomes homeotropically oriented. Smectic germs also turn over if their diameter is below the cell thickness. After the germ has turned over into the homeotropic orientation, one can increase its size by a small decrease of the temperature. Once the germ has become large enough (its lateral dimensions several times the cell thickness) one may turn off the electric field and reach the configuration where a homeotropic smectic germ is in thermal equilibrium with the surrounding ho-

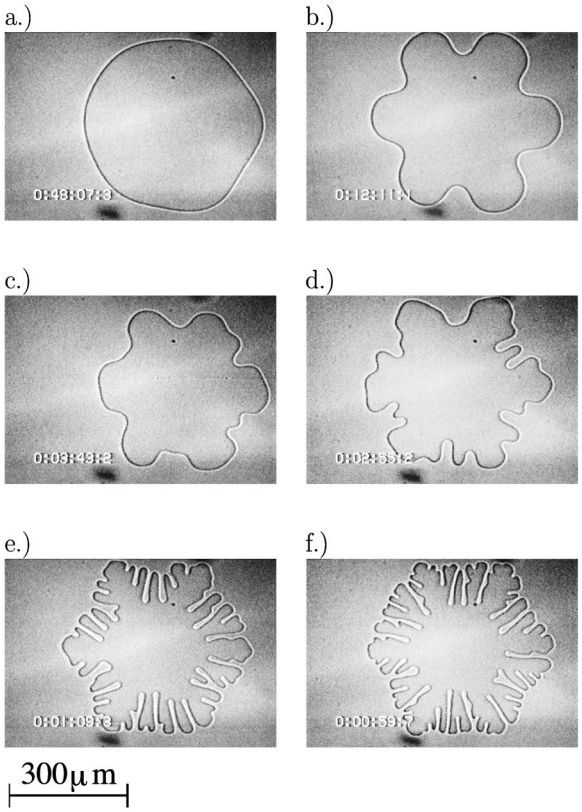

FIG. 1. Growing smectic germs in the undercooled homeotropic nematic (HinH). The corresponding undercooling values are (a)–(f) 0.05 °C, 0.1 °C, 0.12 °C, 0.15 °C, 0.3 °C, and 0.35 °C, respectively. The numbers in the lower left corners of the pictures represent the time elapsed after the onset of undercooling, which are 48 min 7 s, 12 min 11 s, 3 min 43 s, 2 min 55 s, 1 min 9 s, and 59 s, respectively.

meotropic or planar nematic phase (HinH or HinP cases), by adjusting the temperature of the system.

The growth morphologies were detected in a polarizing microscope equipped with a charge coupled device (CCD) camera and an image processing device by applying an undercooling in a range of $0.05°-0.35°$.

III. EXPERIMENTAL RESULTS

HinH configuration: the smectic germ has a nearly circular shape in equilibrium with the homeotropic nematic. From the minimization of the surface energy one expects a hexagonal modulation of the shape due to the symmetry of the smectic-*B* phase [37]. Taking only the first harmonic, the surface tension can be written in the form

$$\tilde{\sigma}(\theta)=1+\frac{\Delta\tilde{\sigma}_6}{2}\cos(6\theta), \tag{3.1}$$

where $\Delta\tilde{\sigma}_6$ is the dimensionless amplitude of the sixfold modulation ($\Delta\tilde{\sigma}_6=\tilde{\sigma}_{\max}-\tilde{\sigma}_{\min}$). The value of $\Delta\tilde{\sigma}_6$ turned out to be extremely small experimentally. Since the shape of the thermally equilibrated interface was found to be practically circular, $\Delta\tilde{\sigma}_6$ has to be smaller than 0.005, which falls within the experimental uncertainty.

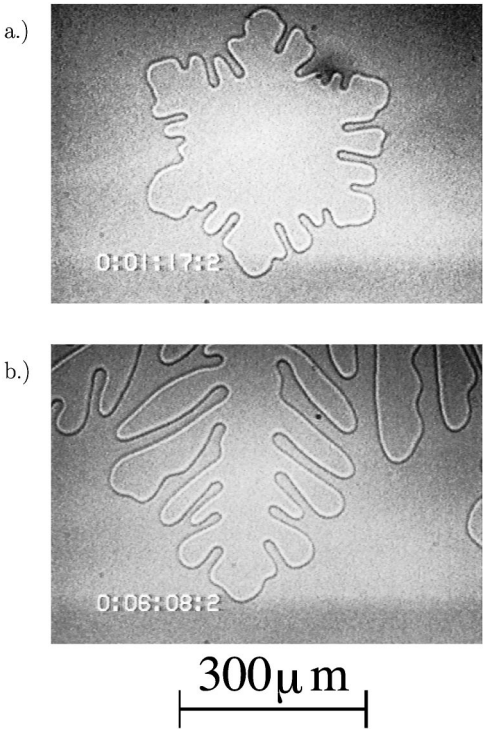

FIG. 2. Dendritic growth of a smectic germ at the undercooling $\Delta T=0.2$ °C (HinH). (a) Snapshot of a germ at $t=1$ min 17 s with six dendritic tips, (b) snapshot of one of the tips at $t=6$ min 8 s, same magnification as in (a).

Preparing a germ in equilibrium and then applying the undercooling one observes the growth of the smectic phase. The experiment was repeated for different undercoolings in the range of $0.05\ °C<\Delta T<0.35\ °C$ using the same germ. In Fig. 1 we show a set of the observed shapes.

One can see that by increasing the undercooling the observed morphology changes from the surface tension stabilized hexagonal through a petal shape into the dendritic and the dense branching regime. The above morphological sequence is in good agreement with the morphological phase diagrams predicted in [38,16]. Note that at large undercooling the envelope of the interface exhibits a hexagonal shape with the same orientation of the long and short axes as in equilibrium.

Dendrites have been seen in a narrow range of undercooling falling between 0.15 °C and 0.3 °C. An example of the dendritic growth is shown for $\Delta T=0.2$ °C in Fig. 2(a). Figure 2(b) shows one tip which was tracked for more than 6 min.

The above growth morphologies are somewhat different from those reported in [28,39] in the same HinH geometry on the well-studied substance (CCH3). In the present case the hexagonal shape of the enveloping curve of the interface is more pronounced. Moreover a stably growing parabolic tip (dendritic shape) was detected here, which indicates that the relevant material parameters $\Delta\tilde{\sigma}_6$ (and/or $\Delta\tilde{\beta}_6$) are larger in the case of CCH5.

HinP configuration: if a homeotropic smectic germ is surrounded by a planar nematic, one expects on symmetry grounds a contribution of the twofold anisotropy to the surface energy. Thus the expression (3.1) is now replaced by

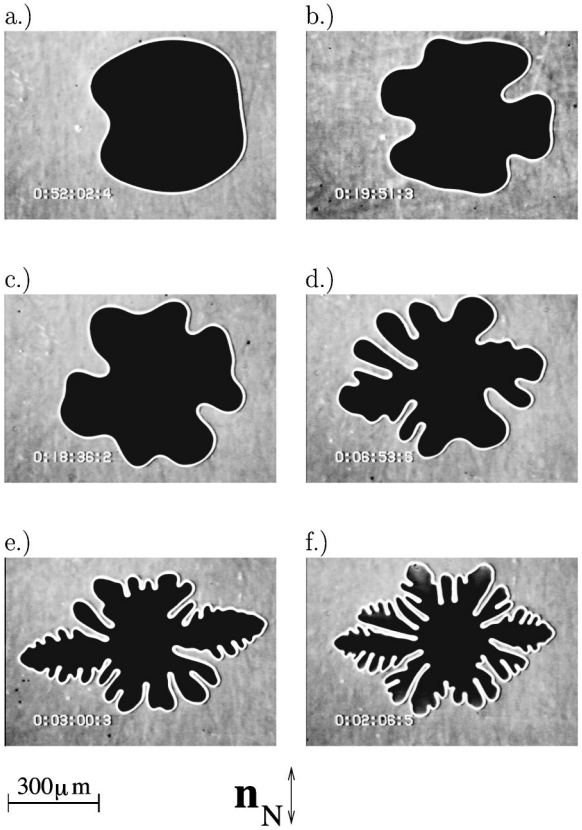

FIG. 3. Growing smectic germs in the undercooled planar nematic (HinP). The nematic director is parallel to y (vertical direction in the figures). The corresponding undercooling values are (a)–(f) 0.05 °C, 0.06 °C, 0.07 °C, 0.1 °C, 0.15 °C, and 0.2 °C, respectively. The numbers in the lower left corners of the pictures represent the time elapsed after the onset of undercooling, which are 52 min 2 s, 19 min 51 s, 18 min 36 s, 6 min 53 s, 3 min, and 2 min 6 s, respectively.

$$\tilde{\sigma}(\theta)=1+\frac{\Delta\tilde{\sigma}_2}{2}\cos(2\theta)+\frac{\Delta\tilde{\sigma}_6}{2}\cos(6\theta). \tag{3.2}$$

The analysis of the observed equilibrium shape (Wulff construction) gives a value for $\Delta\tilde{\sigma}_2$ in the range between -0.02 and -0.06 ($\Delta\tilde{\sigma}_2$ is negative, because the reference direction x has been chosen perpendicular to $\mathbf{n_N}$).

The result that $|\Delta\tilde{\sigma}_2|$ is much larger than $|\Delta\tilde{\sigma}_6|$ can be understood from the fact that in $\Delta\tilde{\sigma}_2$ an elastic energy from the deformation zone between the two phases, where the planar nematic orientation changes to the homeotropic, is involved. Depending on the angle between the surface normal and the nematic director the principle deformations (twist, bend, and splay) contribute differently to this energy.

The same set of experiments (as in the HinH case) was repeated for undercoolings in a similar range of ΔT. In Fig. 3 we show a set of the observed shapes.

One can see that for small undercoolings the morphologies are similar (apart from the fact that the shapes are more irregular) to the HinH case, but at larger ones — where the dendrites should develop — the growth and stabilization of the dendritic tips is suppressed in the direction parallel to $\mathbf{n_N}$ and enhanced in the direction perpendicular to it [see Figs. 3(e) and 3(f)]. We note that the long axis of the enveloping oval shape of the pattern turns over by 90° as a function of the driving force [compare Figs. 3(a) and 3(f)] similar to the observation in viscous fingering experiments in planar smectic liquid crystals [40,41]. In this respect the dependence of the twofold shape modulation on undercooling is different from the sixfold one, as observed in the HinH germs. Another peculiarity is that at undercoolings $\Delta T\geqslant 0.2$ °C in some parts of the growing germ (with surface normal close to the y direction) one has imperfect extinction indicating that the orientation of the smectified substance deviates from the homeotropic [e.g., in Fig. 3(f), upper parts of the smectic phase]. Probably in this regime the time available for a molecule to be attached to the growing crystal ($2-5\times10^{-5}$ s as inferred from the observed velocity) becomes comparable to the typical times of the molecular rotation.

IV. ESTIMATE OF THE RELEVANT ANISOTROPIES FROM NUMERICAL SIMULATIONS OF A PHASE-FIELD MODEL

It was shown in several recent papers that phase-field models provide a useful basis when describing diffusion limited processes, e.g., crystallization [21,42]. A good reproduction of experimentally observed shapes of a crystal growing under well-controlled conditions was reported by using this model and including the experimentally determined material parameters [43,27,29]. In the model a new parameter ϕ, the ''*phase field*,'' describes the difference between the two phases being $\phi=1$ and $\phi=0$ corresponding to the nematic and smectic phases, respectively. It is the basic feature of phase-field descriptions that ϕ changes continuously in space forming a boundary layer between the solid and liquid phases. This variation is rapid but smooth in the vicinity of T_m. We mention that in the limit of zero interface thickness this leads to the sharp interface description which could be interpreted as a jump in ϕ. The dynamics of ϕ is derived from the variation of a Ginzburg-Landau type free energy functional. We use a set of equations derived in [44], where the dynamics satisfies a locally positive entropy production, resulting in the correct latent heat production. In addition we have included in the model the anisotropic heat diffusion which is relevant in the HinP case. The pair of coupled equations for the phase field $\phi(\mathbf{r},t)$ and dimensionless temperature $u(\mathbf{r},t)$ can be written in dimensionless units introduced before as follows:

$$\begin{aligned}\epsilon^2\tau_0\tilde{\beta}(\theta)\tilde{\sigma}(\theta)\,\frac{\partial\phi}{\partial t}=&\,\phi(1-\phi)\left(\phi-\frac{1}{2}+30\epsilon\alpha\Delta u\,\phi(1-\phi)\right)\\&-\epsilon^2\frac{\partial}{\partial x}\left(\tilde{\sigma}(\theta)\tilde{\sigma}'(\theta)\frac{\partial\phi}{\partial y}\right)\\&+\epsilon^2\frac{\partial}{\partial y}\left(\tilde{\sigma}(\theta)\tilde{\sigma}'(\theta)\frac{\partial\phi}{\partial x}\right)\\&+\epsilon^2\nabla[\tilde{\sigma}^2(\theta)\nabla\phi],\end{aligned} \tag{4.1}$$

$$\frac{\partial u}{\partial t}+\frac{1}{\Delta}\,30\phi^2(1-\phi)^2\frac{\partial\phi}{\partial t}=\tilde{D}_i\nabla_i^2 u. \tag{4.2}$$

The first term on the right hand side of Eq. (4.1) can be written as $-d\mu/d\phi$, where the potential $\mu(\phi)$ has minima at $\phi=1$ and $\phi=0$. The potential depends parametrically on u. For $u<0$ the minimum at $\phi=1$ is lower than the one at $\phi=0$ (and vice versa). The equation describes the evolution of the system to the lower minimum in the presence of a sufficiently large germ. The heat diffusion equation (4.2) includes a source term that describes the latent heat production. [Note that in the Ginzburg-Landau description of phase transitions the traditional choice of the analogous (order) parameter would be $\psi=1-\phi$, such that $\psi=1$ in the more ordered phase. In order to be consistent with previous work [44] we keep ϕ.] θ is the angle between the x axis and the gradient of the phase field. The additional dimensionless parameters of the model are

$$\epsilon=\frac{\delta}{\omega}, \quad \tilde{D}_i=\frac{D_i}{D_\perp}, \tag{4.3}$$

where δ is the interface thickness. The sharp-interface description is recovered from the phase-field model in the limit where u varies slowly over ϵ. A correction to this asymptotic limit has been derived recently for the kinetic term [45]. Since in our experiments the director of the smectic phase is always perpendicular to the bounding plates the heat diffusion in this phase is supposed to be isotropic in the plane of the layer (xy plane) with the (dimensionless) diffusion coefficients $\tilde{D}_x=\tilde{D}_y=1$. In the planar nematic phase one has anisotropic heat diffusion in the xy plane with the principle-axis diffusion coefficients $\tilde{D}_x=1$ and $\tilde{D}_y=1+D_a$ if the director is parallel to the y direction (see Fig. 3). Since we assume the heat diffusion coefficients to be the same in both phases the change in the heat diffusion coefficient at the interface comes from the change in the orientation of the director. Having a thin interfacial region in the xy plane, the heat diffusion should change at the phase boundary from isotropic to anisotropic continuously in space with ϕ. Thus we set

$$\tilde{D}_x=1, \quad \tilde{D}_y=1+D_a\phi. \tag{4.4}$$

Since the temperature of the system varies in a narrow range below the phase transition temperature (small undercoolings), we neglect the temperature dependence of the material parameters (including the heat diffusion coefficient) in the simulations.

The two equations (4.1) and (4.2) were solved on a square lattice of 800×800 grid points. In order to ensure numerical stability Eq. (4.2) has been solved using the alternating direction implicit (ADI) method. Since the phase transition takes place at the interface, and the time derivative of the temperature field in Eq. (4.2) is small far away from the interface, one could reduce the computational time by solving only Eq. (4.2) far from the crystal phase on a ''rough'' lattice while taking $\phi=1$ there, and solving both equations on a fine scale in the remaining region. We have chosen a critical value $u_c=-0.9$. For $u<u_c$ we used a rough lattice while for $u>u_c$ we solved both equations on a fine lattice. Of course at the boundary of these two regions one has to match the value of u.

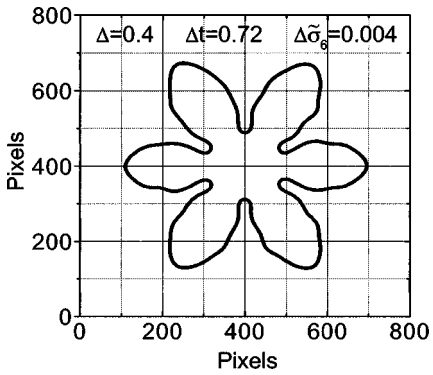

FIG. 4. The shape of a growing crystal with hexagonal surface tension anisotropy and isotropic linear kinetic term. Pixel size $\Delta x=\Delta y=0.005$.

Initial conditions were chosen as follows: $\phi=1$, $u=-1$ all over the two-dimensional (2D) space but one pixel with $\phi=u=0$ in the center of the system. This initial state relaxes after a transient into a configuration where both parameters (u and ϕ) are continuous in space near the phase boundary. Since the system is in contact with an undercooled thermal bath at its boundaries (where $\phi=1$, $u=-1$) the phase transition front moves outwards from the center. The only heat source in the system is the latent heat, which is released at the perimeter of the germ. This heat production acts against the effect of the surrounding thermal bath thus preventing the germ from cooling down and keeping it nearly isothermal near $u=0$.

The fine spatial discretization was chosen as $\Delta x=\Delta y=0.005$ while the time step was $\Delta t=0.0001$. The phase-field constants were $\alpha=350$, $\epsilon=0.005$, $\tau=20$, the mesh spacing of the ''rough'' lattice was $10\,\Delta x$. These parameters including the relevant range of Δ were adjusted in an analogous simulation carried out for the planar germ of the same substance [29,27]. For computational reasons, the simulated germs were about one to two orders of magnitude smaller than the experimental ones. (The exact size in physical units depends on the capillary length d_0, which is unknown because σ_0 is not known.) To partially compensate this difference in size the undercooling in the simulations has to be taken larger than in the experiments.

Actually there is no strict scaling of Eqs. (1.4), (1.5) or (4.1), (4.2) connecting the germ size, expressed in dimensionless units by α [see Eq. (1.9)], with the (dimensionless) undercooling Δ. However, if the temperature field is treated adiabatically, i.e., $\partial u/\partial t$ is neglected, then there is the scaling $\Delta\to\gamma\Delta$, $\alpha\to\alpha/\gamma$, $t\to t/\gamma$, $\tau_0\to\tau_0/\gamma$. Treating the temperature field adiabatically appears to reproduce the scenarios qualitatively. The rescaling of the coefficient τ_0 of the kinetic term is at this point of no consequence, since we will use τ_0 as an adjustable parameter.

HinH configuration: in this geometry the surface tension is given by Eq. (3.1). In order to properly choose the value of $\Delta\tilde{\sigma}_6$ we initially disregard the anisotropy of the kinetic effect by taking $\tilde{\beta}(\theta)=1$. Then we should concentrate on the slow growth regime where the growth morphology is dominated by $\tilde{\sigma}(\theta)$.

Taking a value $\Delta\tilde{\sigma}_6=0.004$, just below the upper limit allowed by the experiments, the dendritic character of the

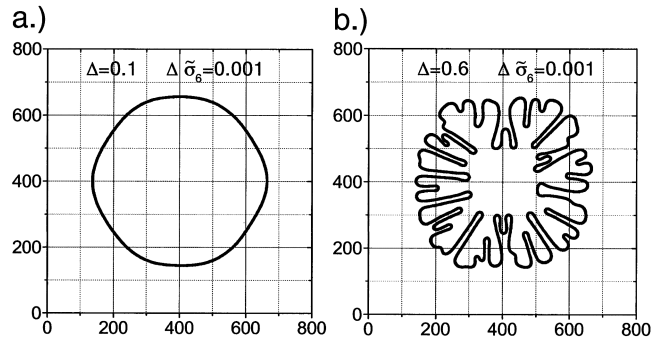

FIG. 5. The shape of growing crystals with hexagonal surface tension anisotropy and isotropic linear kinetic term, using $\Delta\tilde{\sigma}_6 = 0.001$. The units are pixels.

simulated interface was much more pronounced than experimentally observed for any undercooling (compare Fig. 4 with Figs. 1 and 2).

Consequently this is an overestimate of $\Delta\tilde{\sigma}_6$. We reduced the value until we could reproduce the shape of the interface for small undercoolings, which occurred at $\Delta\tilde{\sigma}_6 = 0.001$ [compare Fig. 5(a) with Fig. 1(a)]. For larger undercoolings the hexagonal symmetry of $\sigma(\theta)$ is suppressed by the isotropic kinetics, and the morphology is not reproduced [see Fig. 5(b) and Fig. 1(f)]. In Fig. 5(b) the slight fourfold modulation of the shape results from the anisotropy introduced by the square lattice. Though the corresponding effect of a hexagonal lattice would be smaller, we used the square lattice, because we wanted to ensure that hexagonal shapes are introduced only by the physical effects, e.g., symmetry of the S_B phase. Furthermore, we added spatially and temporally uncorrelated noise with an amplitude of 0.01 to the temperature field $u(r,t)$ in each time step. This perturbation reduces the effect of the fourfold lattice anisotropy. The value of the noise was tuned until its effect smeared the fourfold anisotropy induced by the square lattice.

In order to reproduce the strong hexagonal symmetry of the experimentally observed shapes at larger undercoolings [Figs. 1(e) and 1(f)], we take into account anisotropic kinetics. Considering the experimentally obtained shapes we assume an analogous angular dependence of the kinetic coefficient to that of the surface tension

$$\tilde{\beta}(\theta) = 1 + \frac{\Delta\tilde{\beta}_6}{2}\cos(6\theta). \tag{4.5}$$

Using Eqs. (4.5) and (3.1) we get from Eq. (1.7)

$$u_{\text{interface}} = -\frac{\sqrt{2}}{12\alpha\Delta}\left\{\left(1 - \frac{35}{2}\Delta\tilde{\sigma}_6\cos(6\theta)\right)\kappa + \tau_0\left(1 + \frac{1}{2}\Delta\tilde{\beta}_6\cos(6\theta)\right)v_n\right\}, \tag{4.6}$$

which indicates that in case of $\Delta\tilde{\sigma}_6 > 0$ one needs $\Delta\tilde{\beta}_6 < 0$ in order to reproduce the experimentally observed orientation of the hexagon (as mentioned before, there was no change in the orientation of the hexagonal enveloping boundary curve of the germ with increasing ΔT, contrary to [46]). The magnitude of $\Delta\tilde{\beta}_6$ has been adjusted until the simulation resulted

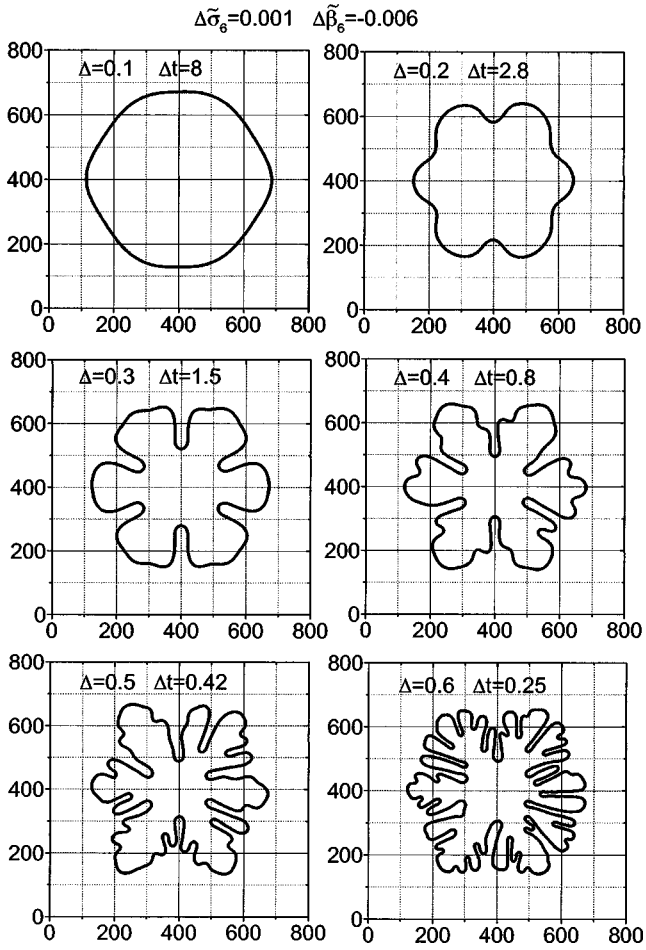

FIG. 6. The shape of growing crystals with hexagonal surface tension anisotropy and hexagonal anisotropic linear kinetic term: $\Delta\tilde{\sigma}_6 = 0.001$ and $\Delta\tilde{\beta}_6 = -0.006$. The value of the dimensionless undercooling (Δ) and the elapsed time are indicated on the pictures. The units are pixels.

in shapes similar to the experiments, which led to $\Delta\tilde{\beta}_6 = -0.006$. Figure 6 shows the numerical results, which are in good qualitative agreement with Fig. 1. We mention that changing the value of the parameters $\Delta\tilde{\beta}_6$ and $\Delta\tilde{\sigma}_6$ by a factor of 2 results in a substantial variation of the shapes obtained by the simulations, which characterizes the typical sensitivity of the method.

We point out that the role of the anisotropic kinetics can be *imitated* in the simulation (artificially) by letting $\Delta\tilde{\sigma}_6$ depend on undercooling. The same set of morphologies as in Fig. 6 can be reproduced by taking isotropic kinetics ($\Delta\tilde{\beta}_6 = 0$) and varying the surface tension anisotropy ($\Delta\tilde{\sigma}_6 = 0.001$, 0.0016, 0.0016, 0.002, 0.002, and 0.004, corresponding to the undercoolings given in Fig. 6). This assumption—though unphysical—supports the choice of the hexagonally symmetric $\tilde{\beta}(\theta)$ function given in Eq. (4.5).

When modeling the *HinP configuration* one should include three additional effects (compared to the HinH geometry) which we will analyze separately.

(1) The twofold contribution $\Delta\tilde{\sigma}_2$. Using the largest anisotropy compatible with the equilibrium-shape measure-

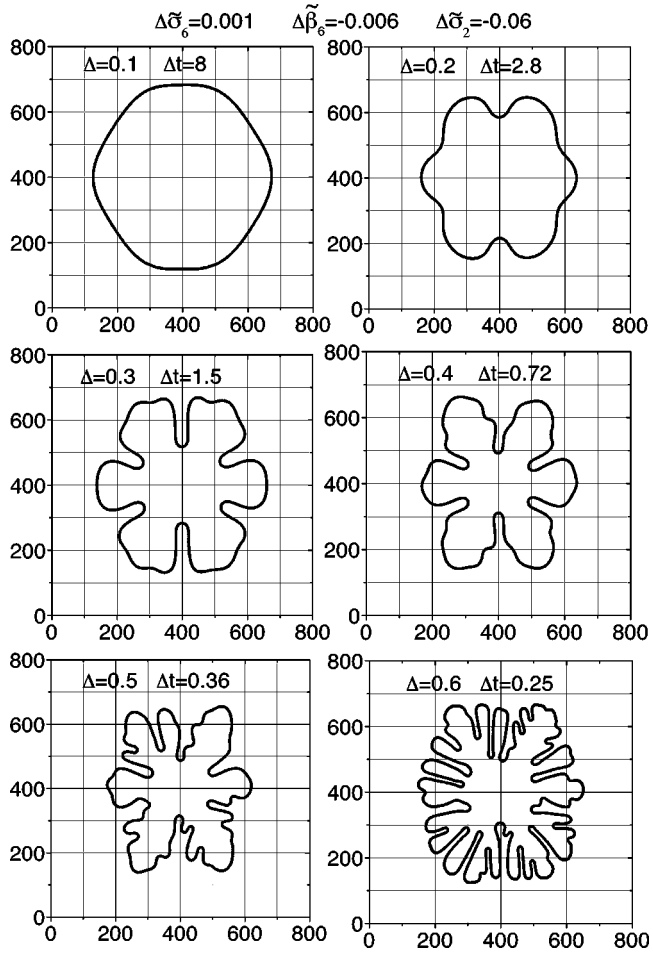

FIG. 7. The shape of growing crystals with hexagonal and twofold surface tension anisotropy and hexagonal anisotropic linear kinetic term: $\Delta\tilde{\sigma}_6=0.001$, $\Delta\tilde{\sigma}_2=-0.06$, and $\Delta\tilde{\beta}_6=-0.006$. The value of the dimensionless undercooling (Δ) and the elapsed time are indicated in the plots. The units are pixels.

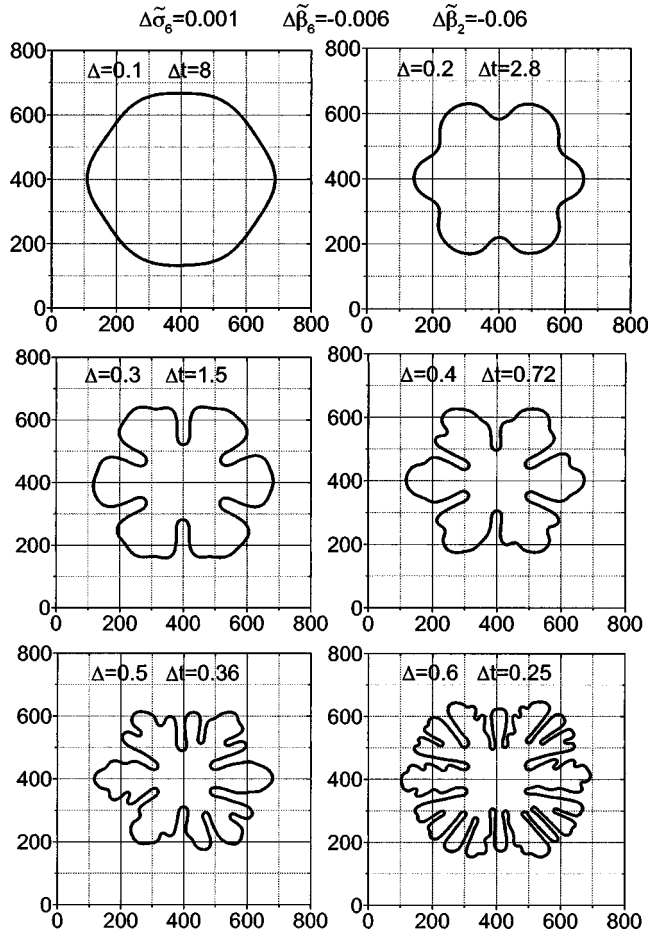

FIG. 8. The shape of growing crystals with hexagonal surface tension anisotropy and hexagonal anisotropic linear kinetic term: $\Delta\tilde{\sigma}_6=0.001$, $\Delta\tilde{\beta}_6=-0.006$, and $\Delta\tilde{\beta}_2=-0.06$. The value of the dimensionless undercooling (Δ) and the elapsed time are indicated in the pictures. The units are pixels.

ments ($\Delta\tilde{\sigma}_2=-0.06$, see above) and the other input parameters the same as in Fig. 6, the numerically obtained shapes are shown in Fig. 7. As can be seen this effect causes an elongation of the growing germ in the direction parallel to the nematic director at any undercooling. Note that the twofold shape anisotropy is still visible at the largest undercooling contrary to the sixfold one, which vanishes; this is probably due to the relatively large value of $\Delta\tilde{\sigma}_2$ compared to $\Delta\tilde{\sigma}_6$ (compare Figs. 5 and 7). Since the experimentally observed shapes show for large ΔT an elongation in the perpendicular direction, a different mechanism has to be operative there.

(2) The kinetics of the phase transformation is supposed to depend on the angle enclosed by the surface normal and the nematic director. This effect can be described by including a twofold modulation of the kinetic term ($\Delta\tilde{\beta}_2$) in analogy to the surface tension. We include a small $\Delta\tilde{\beta}_2$ with negative sign, which will result in an elongation of the growth shape as experimentally observed, and which can also be understood intuitively, as will be seen later (Sec. V). In the absence of experimental information about the magnitude of this effect we use the same amplitude (6%) as in the case of the surface tension modulation. In Fig. 8 the resulting morphologies are shown. In these simulations we have set $\Delta\tilde{\sigma}_2=0$. The twofold modulation of the kinetic term causes a slight elongation of the shape in the direction perpendicular to the nematic director (as observed experimentally), but does not reproduce the rapidly growing two dendrites perpendicular to the nematic director.

(3) As already mentioned in the introduction of the phase-field model, the heat diffusion in the planar nematic layer (the xy plane) is anisotropic. Since in the experiments we have a thin layer of liquid crystal between two glass plates, we should take into account the heat flow through the bounding plates (along z) too. The heat conductivity of the glass plates is of the same order as that of the nematic (and it is isotropic). The effect of the heat flow in the z direction could be modeled by introducing a heat dissipative term (linear with u) into Eq. (4.2) [47]. As it was checked by numerical calculations this term reduces the effect of the heat diffusion anisotropy on the growth shapes. For simplicity we here keep Eq. (4.2) and account for this effect by taking a reduced (effective) value for D_a in the two-dimensional model system. It turned out that the value of $D_a=0.5$ causes a very strong elongation of the enveloping curves of the interface in the direction of x. To demonstrate that a relatively small heat diffusion anisotropy already has an effect on the shape of the

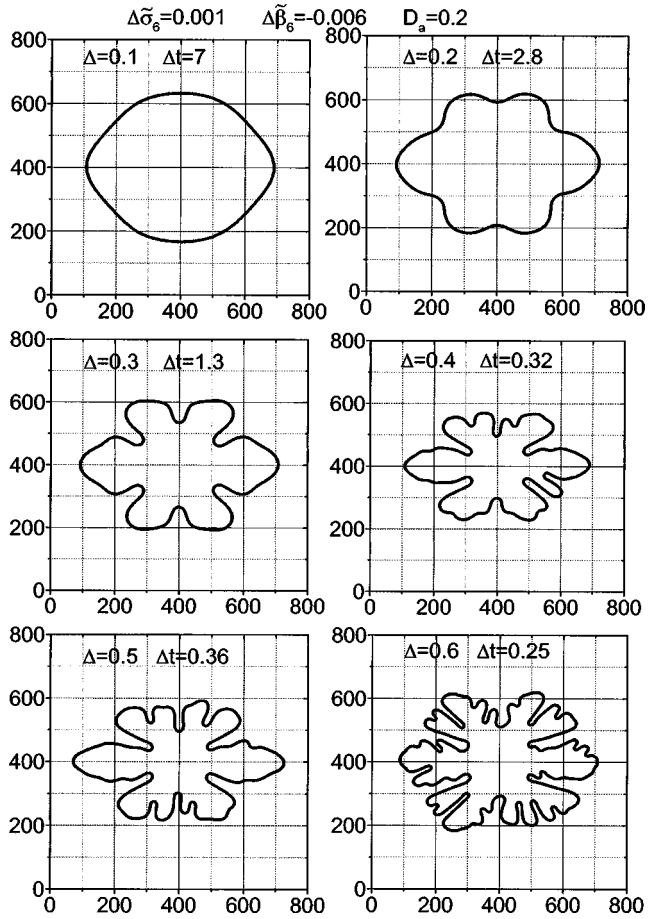

FIG. 9. The shape of growing crystals with hexagonal surface tension anisotropy and hexagonal anisotropic linear kinetic term in the presence of heat diffusion anisotropy in the liquid phase. $\Delta\tilde{\sigma}_6 = 0.001$, $\Delta\tilde{\beta}_6 = -0.006$, and $D_a = 0.2$. The value of the dimensionless undercooling (Δ) and the elapsed time are indicated in the plots. The units are pixels.

growing germs in a pure two-dimensional system, we show the simulation results with $D_a = 0.2$ (and $\Delta\tilde{\sigma}_2 = \Delta\tilde{\beta}_2 = 0$) in Fig. 9. One sees that already at this low value of D_a the heat diffusion anisotropy at any undercooling causes a stronger elongation of the shape than the kinetic effect did, and it is in fact comparable to the effect of $\Delta\tilde{\sigma}_2$ (Fig. 7).

The effect of the heat diffusion anisotropy might appear surprising: those tips move faster which grow in the direction of the smaller heat diffusion (''inverted growth'').

To analyze the problem of the ''inverted growth'' we studied (numerically) a simplified situation in which $\Delta\sigma = 0$ and $\Delta\beta = 0$, the only nonzero anisotropy is $D_a = 0.5$ with $\tilde{D}_x < \tilde{D}_y$. We started with a circular germ in two different initial conditions. (*A*) Steplike temperature and phase field at the interface of the crystal ($u = \phi = 0$ inside the germ and $u = -1$, $\phi = 1$ outside). This assumption could model the experimental case where the germ nucleates in the undercooled nematic. However, one should be aware that this situation can become realistic only after an initial transient during which $u(\mathbf{r})$ is smoothed out and becomes slowly varying over the length ϵ. (*B*) The temperature field u is constant (zero) in the whole system except at the boundaries where it

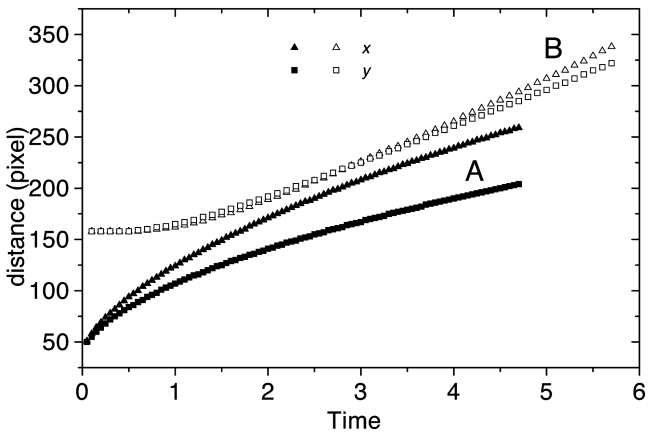

FIG. 10. The distance of the interface as a function of time in two directions (x and y) measured from the center of the starting germ. The initial germs were circular with the radius of 50 (case A) and 160 (case B) grid points, the undercooling values $\Delta = 0.15$ in case A while $\Delta = 0.2$ in case B. The phase field parameters were $\alpha = 315$, $\epsilon = 0.005$, $\tau_0 = 18$. The spatial unit is a pixel.

is set to -1, while ϕ is steplike as in the previous case. Case *B* models the experimental situation when a single germ in equilibrium comes into contact with a colder system at its boundaries.

In Fig. 10 the distance of the interface from the center of the initially circular germ is plotted versus time in the two principle (x and y) directions. Curves *A* and *B* represent the two cases. We chose two different initial radii (50 in case *A* and 160 in case *B*) in order to produce similar sizes in the later stages.

In case *A* the germ becomes elongated in the direction of the smaller heat diffusion coefficient (x) (inverted growth) from the beginning on. In case *B* one has initially ''normal growth,'' i.e., faster in the direction of larger diffusion constant. Subsequently there is a crossover to inverted growth.

To understand the inverted growth it is useful to introduce a coordinate system with rescaled coordinate $y' = (\tilde{D}_x/\tilde{D}_y)^{1/2} y$, while $x' = x$. In this representation diffusion is isotropic, consequently Eqs. (1.5) and (1.6) can be used as they stand for the isotropic case. In Eq. (1.7) κ must be replaced by $s(\theta')\kappa'$ and v_n by $w(\theta')v_n'$, where κ' and v_n' are the curvature and normal velocity in the new coordinates, and

$$s(\theta') = \left(\frac{\tilde{D}_y}{\tilde{D}_x}\right)^{1/2}\left[1 + \left(\frac{\tilde{D}_y}{\tilde{D}_x} - 1\right)\cos^2\theta'\right]^{-3/2},$$
$$w(\theta') = \left[1 + \left(\frac{\tilde{D}_y}{\tilde{D}_x} - 1\right)\cos^2\theta'\right]^{-1/2}. \tag{4.7}$$

[Also in $\tilde{\sigma}(\theta)$ and $\tilde{\beta}(\theta)$ one has to eliminate θ by the relation $\tan\theta = (\tilde{D}_y/\tilde{D}_x)^{1/2}\tan\theta'$.] Thus the effect of the heat diffusion anisotropy can be absorbed, apart from rescaling, in an additional twofold surface tension and kinetic anisotropy with ''easy axis'' along x (for $\tilde{D}_y > \tilde{D}_x$). Clearly this will enhance (speed up) growth in the x direction. In particular, for $\tilde{\sigma} = 1$, the heat diffusion anisotropy alone induces den-

dritic growth in the x direction. This then explains the inverted growth. The observation that under some conditions one has initially a transient normal growth can be explained by the fact that for those conditions it takes some time for the instability to develop. Thus in case B cooling at the boundaries of a square region (in the x, y coordinates) first has to become effective at the location of the germ, so here the better heat diffusion along y dominates the initial evolution.

The effect of the heat diffusion anisotropy has been studied previously in a different geometry (planar smectic in planar nematic) [14] where nonreflection symmetry of the four-armed dendrites was observed experimentally and reproduced numerically. The growth of dendritic tips was also favored in the direction with smaller heat diffusion coefficient.

V. CONCLUDING REMARKS

We found different growth morphologies (among them dendritic) of a growing smectic-B phase in the undercooled nematic, depending on the undercooling in a system with hexagonal symmetry (HinH) with very small surface tension anisotropy. By comparing these morphologies with the results of computer simulations using a phase-field model (including anisotropic surface tension and an anisotropic linear kinetic term) we estimated the value of the amplitude of the sixfold surface tension and kinetic anisotropies. The resulting values are $\Delta\tilde{\sigma}_6 = 0.001$ and $\Delta\tilde{\beta}_6 = -0.006$. The opposite sign of the two parameters $\Delta\tilde{\sigma}_6$ and $\Delta\tilde{\beta}_6$ describes the fact that the six preferred directions in the surface tension dominated and the kinetic regime are the same [see Eqs. (1.6) and (1.7)]. This is in accordance with the assumption that the phase transformation kinetics of the molecules is the slowest on the sides parallel to the hexagonal lattice directions, because it is more difficult to begin to build a new layer, than to continue an existing one at the ''corners.''

On the contrary, in the experiments on columnar hexagonal liquid crystals [25] the hexagonal shapes of the crystal at low (surface tension controlled regime) and at high (kinetic regime) undercoolings were rotated by 30° with respect to each other, which means that the sign of the two parameters $\Delta\tilde{\sigma}_6$ and $\Delta\tilde{\beta}_6$ was the same. However, the magnitude of the anisotropies reported in [25] ($\Delta\tilde{\beta}_6 = 1.12\times10^{-2}$ and $\Delta\tilde{\sigma}_6 = 6\times10^{-3}$) is similar to our result.

The HinP geometry must be induced by an external electric field since in most cases (for several different substances) the smectic phase nucleates in the form of planar (or tilted) germs even in cells with homeotropic orientation [27,39]. Elongated growth shapes of the smectic germs were found. For small undercooling the long axis of their enveloping curve was parallel to the nematic director, while at large undercooling it was found perpendicular to the director. In the last case the development of stable dendritic tips along the long axis of the enveloping curve is favored, whereas it is suppressed in the direction parallel to the nematic director. In the development of these elongated shapes apparently three effects act simultaneously: (1) the twofold modulation of the surface tension of the nematic–smectic-B interface, (2) the phase transformation kinetics where one should take into account the reorientation of the molecules during the crystallization process, and (3) the anisotropic heat diffusion in the nematic phase.

Since the long and short axes of the twofold shape anisotropy interchange with increasing undercooling the signs of $\Delta\tilde{\beta}_2$ and $\Delta\tilde{\sigma}_2$ (<0, see above) must be the same [see Eqs. (1.6) and (1.7)]. Thus, when the surface is oriented parallel to the nematic director so that the reorientation of the director involves mainly twist (low-surface tension part), the kinetics should be faster than when the reorientation involves mainly splay. This appears indeed plausible because the evolution of a twist distortion involves no backflow, in contrast to the evolution of splay [48]. Alternatively, on the molecular level, one might argue that the development of the twisted interface involves only rotation of molecules, whereas in the development of the splayed part most of the rodlike molecules additionally have to undergo a center-of-mass motion.

The effect of anisotropy of heat diffusion is to induce, possibly after an initial transient, faster growth of a germ in the direction of low heat diffusion. Also dendritic growth is favored in this direction.

Comparing these three effects at finite undercooling we found that the actual surface tension modulation acts oppositely compared to the other two. At not too small undercooling both the kinetic and the diffusion anisotropy result in similar shapes as observed experimentally. In order to separate the two, further measurements should be done to determine the kinetic anisotropy and the actual heat diffusion anisotropy in the specified geometry.

ACKNOWLEDGMENTS

The authors wish to thank T. Tóth-Katona and R. González-Cinca for fruitful discussions. The work was financially supported by the EU TMR under Project No. ERB FMRX-CT 96-0085, by the Hungarian National Research Fund under Grant No. OTKA T014957, and the Volkswagen Foundation.

[1] *Solids far from Equilibrium*, edited by C. Godrèche (Cambridge University Press, Cambridge, England, 1992).
[2] J. Langer, in *Chance and Matter*, Les Houches, Session XLVI, edited by J. Souletie *et al.* (Elsevier, Amsterdam, 1987).
[3] E. Rubinstein and M. Glicksman, J. Cryst. Growth **112**, 97 (1991).
[4] E. Rubinstein and M. Glicksman, J. Cryst. Growth **112**, 84 (1991).
[5] A. Dougherty, J. Cryst. Growth **110**, 501 (1991).
[6] K. Koo, R. Ananth, and W. Gill, Phys. Rev. A **44**, 3782 (1991).
[7] M. Muschol, D. Liu, and H. Cummins, Phys. Rev. A **46**, 1038 (1992).
[8] M. Glicksmann and N. Singh, J. Cryst. Growth **98**, 277 (1989).
[9] A. Dougherty and J. Gollub, Phys. Rev. A **38**, 3043 (1988).
[10] A. Shalnikov Zh. Éksp. Teor. Fiz. **41**, 1059 (1961) [Sov. Phys.

JETP **14**, 755 (1962)].
[11] B. Fraass, S. Heald, and R. Simmons, J. Cryst. Growth **42**, 370 (1977).
[12] D. Temkin, J. Géminard, and P. Oswald, J. Phys. I **4**, 403 (1994).
[13] E. Raz, S. Lipson, and E. Polturak, Phys. Rev. A **40**, 1088 (1989).
[14] R. González-Cinca, L. Ramírez-Piscina, J. Casademunt, A. Hernández-Machado, T. Tóth-Katona, T. Börzsönyi, and Á. Buka, J. Cryst. Growth **193**, 712 (1998).
[15] E. Ben-Jacob and P. Garik, Physica D **38**, 16 (1989).
[16] E. Ben-Jacob and P. Garik, Nature (London) **343**, 523 (1990).
[17] O. Shochet, K. Kassner, E. Ben-Jacob, S. Lipson, and H. Müller-Krumbhaar, Physica A **181**, 136 (1992).
[18] H. Müller-Krumbhaar, in *Morphology of Crystals*, edited by I. Sunagawa (Terra Scientific Publishing Company, Tokyo, 1987).
[19] O. Shochet, K. Kassner, E. Ben-Jacob, S. Lipson, and H. Müller-Krumbhaar, Physica A **187**, 87 (1992).
[20] E. Brener, M. Gellikman, and D. Temkin, Zh. Éksp. Teor. Fiz. **94**, 241 (1988) [Sov. Phys. JETP **67**, 1003 (1988)].
[21] A. Wheeler, B. Murray, and R. Schaefer, Physica D **66**, 243 (1993).
[22] G. McFadden, A. Wheeler, R. Braun, S. Coriell, and R. Sekerka, Phys. Rev. E **48**, 2016 (1993).
[23] J. Bechhoefer, in *Pattern Formation in Liquid Crystals*, edited by L. Kramer and Á. Buka (Springer-Verlag, New York, 1996).
[24] P. Oswald, J. Malthéte, and P. Pelcé, J. Phys. (Paris) **50**, 2121 (1989).
[25] J. Géminard, P. Oswald, D. Temkin, and J. Malthête, Europhys. Lett. **22**, 69 (1993).
[26] J. Hutter and J. Bechhoefer, Physica A **239**, 103 (1997).
[27] T. Tóth-Katona, T. Börzsönyi, Z. Váradi, J. Szabon, Á. Buka, R. González-Cinca, L. Ramírez-Piscina, J. Casademunt, and A. Hernández-Machado, Phys. Rev. E **54**, 1574 (1996).
[28] Á. Buka, T. Tóth-Katona, and L. Kramer, Phys. Rev. E **51**, 571 (1995).
[29] R. González-Cinca, L. Ramírez-Piscina, J. Casademunt, A. Hernández-Machado, L. Kramer, T. Tóth-Katona, T. Börzsönyi, and Á. Buka, Physica D **99**, 359 (1996).
[30] W. Urbach, H. Hervet, and F. Rondelez, J. Chem. Phys. **78**, 5113 (1983).
[31] M. Marinelli, F. Mercuri, S. Foglietta, U. Zammit, and F. Scudieri, Phys. Rev. E **54**, 1604 (1996).
[32] M. Marinelli (private communication).
[33] M. Marinelli, F. Mercuri, U. Zammit, and F. Scudieri, Phys. Rev. E **53**, 701 (1996).
[34] U. Zammit, M. Marinelli, R. Pizzoferrato, F. Scudieri, and S. Martellucci, Phys. Rev. A **41**, 1153 (1990).
[35] U. Zammit, M. Marinelli, R. Pizzoferrato, F. Scudieri, and S. Martellucci, Liq. Cryst. **4**, 619 (1989).
[36] F. Rondelez, W. Urbach, and H. Hervet, Phys. Rev. Lett. **41**, 1058 (1978).
[37] G. Gray and J. Goodby, *Smectic Liquid Crystals* (Leonard Hill, Glasgow, 1984).
[38] E. Brener, H. Müller-Krumbhaar, and D. Temkin, Phys. Rev. E **54**, 2714 (1996).
[39] T. Tóth-Katona and Á. Buka, Mol. Cryst. Liq. Cryst. Sci. Technol., Sect. A **261**, 349 (1995).
[40] Á. Buka and P. Palffy-Muhoray, J. Phys. (France) **49**, 1319 (1988).
[41] V. Horváth, J. Kertész, and T. Vicsek, Europhys. Lett. **4**, 1133 (1987).
[42] R. Kobayashi, Physica D **63**, 410 (1993).
[43] B. T. Murray, A. A. Wheeler, and M. E. Glicksman, J. Cryst. Growth **154**, 386 (1995).
[44] S.-L. Wang, R. Sekerka, A. Wheeler, B. Murray, R. Braun, S. Coriell, and G. McFadden, Physica D **69**, 189 (1993).
[45] A. Karma and W.-J. Rappel, Phys. Rev. E **53**, R3017 (1996).
[46] P. Oswald, J. Phys. (Paris) **49**, 1083 (1988).
[47] G. Shalaby, Ph.D. thesis, Menofia University, Egypt, 1996.
[48] S. Chandrasekhar, *Liquid Crystals* (Cambridge University Press, Cambridge, England, 1992).